High-efficiency SO_2 removal on Fe-impregnated activated carbon fiber-oxidized using low-concentration oxygen gas

Huda, Miftahul
Research Center for Mineral Technology, National Research and Innovation Agency (BRIN)

Monika, Ika
Research Center for Mineral Technology, National Research and Innovation Agency (BRIN)

Suganal, Suganal
Research Center for Mineral Technology, National Research and Innovation Agency (BRIN)

Daulay, Amru
Research Center for Mineral Technology, National Research and Innovation Agency (BRIN)

他

出版情報：Carbon Trends. 21, pp.100570-, 2025-12. Elsevier
バージョン：

Carbon Trends 21 (2025) 100570

Contents lists available at ScienceDirect

Carbon Trends

journal homepage: www.elsevier.com/locate/cartre

High-efficiency SO_2 removal on Fe-impregnated activated carbon fiber-oxidized using low-concentration oxygen gas

Miftahul Huda [a,*], Ika Monika [a], Suganal Suganal [a], Amru Daulay [a], Edwin Akhdiat Daranin [a], Teuku Ishlah [b], Jin Miyawaki [b,c,d]

[a] Research Center for Mineral Technology, National Research and Innovation Agency (BRIN), Jl. Ir. Sutami, Km. 15, Tanjung Bintang, South Lampung, Lampung Province, Indonesia
[b] Research Center for Geological Resources, National Research and Innovation Agency (BRIN), Jalan Cisitu, Sangkuriang Bandung, Jawa Barat 40135, Indonesia
[c] Interdisciplinary Graduate School of Engineering Sciences, Kyushu University, 6-1 Kasuga-koen, Kasuga, Fukuoka, 816-8580, Japan
[d] Institute for Materials Chemistry and Engineering, Kyushu University, 6-1 Kasuga-koen, Kasuga, Fukuoka, 816-8580, Japan

ARTICLE INFO

Keywords:
Activated carbon
SO_2 removal
Fe-impregnated
Active carbon fiber

ABSTRACT

Carbon-based adsorbents exhibit strong adsorption capabilities for low-concentration SO_2, and thus exhibit high-efficiency removal performance of SO_2 from exhaust gas. This study aims to further improve the SO_2 adsorption capacity of pitch-based activated carbon fiber (ACF) through controlled oxidation. Pristine ACF (PACF) and Fe-impregnated ACF (FeACF) were oxidized using low-concentration oxygen gas (2 % O_2 in N_2). The results showed that the oxidation of ACFs using low concentration O_2 increased the contents of oxygen-containing surface functional groups, and the oxidation of ACFs followed by heat treatment increased the specific surface area and widened the pore size. The adsorption capacity of PACF was 150.8 mL/g-ACF. Oxidization of FeACF at 450 °C for 1 hour and heat treatment at 1100 °C increased the SO_2 removal capacity, reaching 491.0 mL/g-ACF.

1. Introduction

Sulfur dioxide (SO_2) emission standards from coal-fired power plants (CFPPs) worldwide are increasingly tightened, forcing CFPPs to improve the efficiency of their pollutant removal processes, which results in increased costs [1]. The operating cost of the flue gas desulfurization (FGD) process in China will increase from CNY 64.8 billion to CNY 78.6 billion if the desulfurization efficiency is increased from 98 % to 99 % [2]. SO_2 in flue gas is currently removed by wet scrubber systems with calcium hydroxide slurries. Alternative desulfurization technologies must be developed to reduce costs and meet emission standards.

Carbon-based adsorbents are considered a promising and economical technology for flue gas desulfurization because they use simple equipment, are easy to operate, and cause less secondary pollution [3]. The adsorption method exhibits strong adsorption capabilities for low-concentration exhaust gases [4]. Therefore, it may be combined with low-efficiency desulfurization technology to achieve deep purification at a lower cost. A process of desulfurization system combining low-efficiency limestone injection into the furnace and activated carbon (AC) adsorption in the rear of the gas purification system has also been proposed as a method to achieve ultra-low SO_2 emission in a circulating fluidized bed coal-fired boiler [5].

Among carbon-based adsorbents, active carbon fiber (ACF) is an adsorbent that has the highest activity against SO_2 [6]. The by-product H_2SO_4 can be removed from the ACF. It can recover the active ACF site and be further used for desulphurization. Heat treatment of ACF increases its adsorption capacity since heat treatment that evolves CO and CO_2 raises the number of active sites and improves surface basicity. Therefore, increasing active site density is a key step for enhancing SO_2 adsorption capacity. Recently, some advanced methods have been developed to increase the active site density of catalysts [7–9]. Here, we used a simple method, oxidation followed by calcination, to modify the ACF surface to increase its active site density. Oxidation is one of the most conventional modifications used for ACs. It is mainly used to introduce carbon-oxygen surface groups in AC.

Oxidation methods involve the utilization of oxidizing gases (O_2, H_2O, CO_2) or oxidizing solutions (HNO_3, H_2O_2, Cl). The AC's dry and wet oxidation treatments used O_2, HNO_3, and H_2O_2 [10]. Oxidation using air for coal [11], pitch-based ACF [12–14], and biochar [15]. It shows the increase in specific surface area and the average width of

* Corresponding author.
E-mail address: mift013@brin.go.id (M. Huda).

https://doi.org/10.1016/j.cartre.2025.100570
Received 23 July 2025; Received in revised form 31 August 2025; Accepted 12 September 2025
Available online 15 September 2025

micropores. However, air oxidation is difficult to control, which can lead to ignition [16]. Ignition reaction is a violent exothermic reaction of carbon with oxygen, drastically decreasing the adsorbent weight. Uncontrolled oxidation using HNO_3 destroys the pore walls of AC to yield a lower surface area. HNO_3 destroys the pore walls of the AC prepared from olive stone to yield a lower surface area [17]. The SEM study after oxidation with HNO_3 demonstrated the erosive effect of HNO_3 in disintegrating the carbon grains and enlarging macropores [18]. However, the surface area may be recovered after heat treatment, and a high surface area may be produced when the precursor is coal [19,20].

This study aims to develop an oxidation method for pitch-based ACF to improve its SO_2 adsorption capacity. Low oxygen concentration gas (LOG) containing a mixture of N_2 and O_2 will be used. The oxidation conditions will be optimized to prevent ignition so that the oxygen content and surface area of ACFs increase. The role of iron nitrate impregnated in ACF (FeACF) will be studied to understand the role of iron on the oxidation rate and SO_2 adsorption capacity of ACF. The current authors have studied using LOG with an oxygen concentration of about 6 % to minimize uncontrolled exothermic heating in combustion experiments to measure coal reactivity [21]. Oxidation conditions consisting of O_2 concentration and temperature were optimized to determine the difference in oxidation reactivity of coal and ACF.

2. Experimental

2.1. Materials

Pitch-based active carbon fiber was obtained by Osaka Gas Co. (OG15A). Iron (III) nitrate enneahydrate ($Fe(NO_3)_3.9H_2O$) was obtained from Wako. SO_2, O_2, and N_2 were obtained by local distribution in Japan.

2.2. Synthesis of feacf

Pristine ACF (PACF) was dried in a vacuum oven at 120 °C. Then, adding $Fe(NO_3)_3{\cdot}9H_2O$ solution in a weight ratio of metal and ACF of 0.5 % for six hours. Solids were obtained by filtering while washing with ethanol. The solids were dried in the oven. This sample was named FeACF.

2.3. Oxidation of ACFs

PACF and FeACF were oxidized at different temperatures and times in a vertical tube furnace equipped with a gas distributor using 21 %, 6 %, and 2 % O_2 in N_2. The gas flow rate and the amount of ACF in each oxidation were 1 L/min and 1 g, respectively. The samples are named according to Table 1.

2.4. Heat treatment of ACFs

All ACFs were heat-treated to remove oxygen from their surfaces before SO_2 removal experiments. It has been reported that polyacrylonitrile, coal tar pitch, and ethylene tar pitch-based ACFs showed the highest activity for SO_2 removal after calcination at 800 °C [6], 1100 °C [22] and 1100 °C [23,24], respectively. Heat treatment promotes the rearrangement of carbon chains into a more graphitic structure. As a result, it enhances electrical conductivity, thermal stability, and chemical stability [25]. The SO_2 adsorption capacity of coal tar pitch-based ACF decreased upon calcination above 1100 °C, although the basicity properties remained increased [24]. This may be due to a decrease in micropores or specific surface area after calcination at a higher temperature. Therefore, the heat treatment temperature of ACFs was set at 1100 °C in this study. The heat treatments were conducted under argon gas at a heating rate of 10 °C/min and a furnace temperature of 1100 °C without holding time. About 300 mg ACF was used in each heat treatment, and the weight loss after heat treatment was measured.

2.5. SO_2 removal experiment

The apparatus used for the SO_2 removal experiment is illustrated in Fig. 1. The adsorption was conducted by flowing a simulated flue gas containing 1000 ppmv SO_2, 5 % volume of O_2, and 10 % volume of H_2O in N_2 into a reaction tube with an ACF bed inside. The Flame Photometric Detector (FPD) continuously measured the concentrations of SO_2 at the tube outlet. Each experiment uses 0.1 g of ACF. It is packed in a reaction tube of 8 mm diameter at a packing density of about 0.1 g/cm. The ACF's bed temperature was maintained at 50 °C using an electric heater. The experimental procedure has been described elsewhere [6, 22].

2.6. Characterization of ACFs

ACFs were characterized their morphology, pore properties, weight loss during heating, and surface chemistry to understand their influence on SO_2 adsorption. The morphology was examined by scanning electron microscope (SEM). Pore properties of ACFs were determined by Sorptomatic 1990 using nitrogen gas at 77 K. TG/DTA (Seiko 220) was used to measure ACF weight loss under an inert atmosphere using ACF of particle size smaller than 75 mm, the weight of 5 mg + 0.1 mg, and a heating rate of 15 °C/min. The surface oxygen-containing functional groups on the ACF were characterized by temperature-programmed desorption (TPD). It was carried out by heating 50 mg samples under helium gas flow at a heating rate of 10 °C/min up to 1000 °C to analyze the evolved gases continuously, such as CO and CO_2, by the quadrupole mass spectrometer.

3. Results and discussion

3.1. Oxidization of ACF

The yield of PACF and FeACF at different oxidation conditions can be seen in Fig. 2. Generally, the yield of oxidized ACF decreases under more severe oxidation conditions (reaction time, temperature, or O_2 concentration). PACF suffered a low yield (43 %) during oxidation at a temperature of 420 °C under a flow of air (PACF-ox21 %T42) for one hour. A significant increase in PACF bed temperature was also observed during

Table 1
The list of notations used in this paper.

Materials	Oxidation conditions			Notation	Materials	Oxidation conditions			Notation
	O_2 (%)	T (oC)	t (hour)			O_2 (%)	T (oC)	t (hour)	
PACF	21	420		PACF-ox21 %T42	FeACF	2	400		FeACF-ox2 %T40
PACF	6	400		PACF-ox6 %T40	FeACF	2	350		FeACF-ox2 %T35
PACF	6	500		PACF-ox6 %T50	FeACF	2	450		FeACF-ox2 %T45
PACF	2	550		PACF-ox2 %T55	FeACF	2	300	1	FeACF-ox2 %T30t1
PACF	2	550	0.5	PACF-ox2 %T55t0.5	FeACF	2	350	1	FeACF-ox2 %T35t1
PACF	2	550	1	PACF-ox2 %T55t1	FeACF	2	400	1	FeACF-ox2 %T40t1
PACF	2	550	2	PACF-ox2 %T55t2	FeACF	2	450	1	FeACF-ox2 %T45t1
PACF	2	550	3	PACF-ox2 %T55t3					

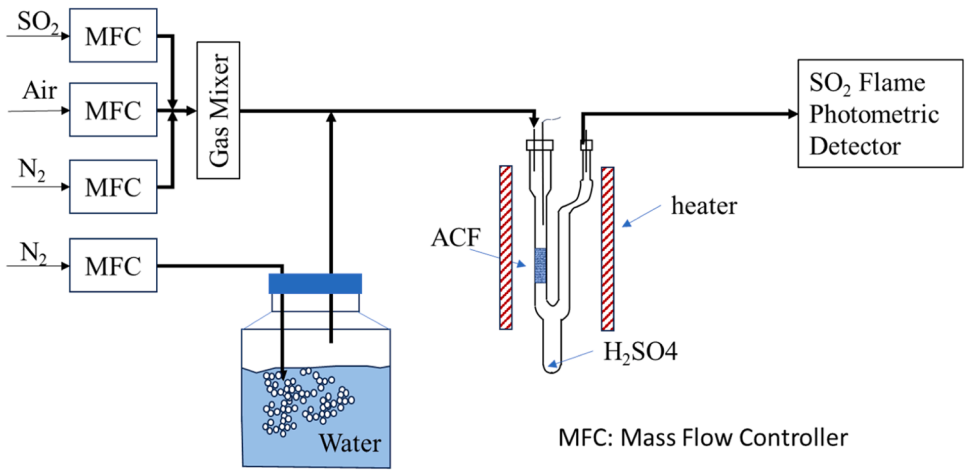

Fig. 1. Flow diagram of the experiment.

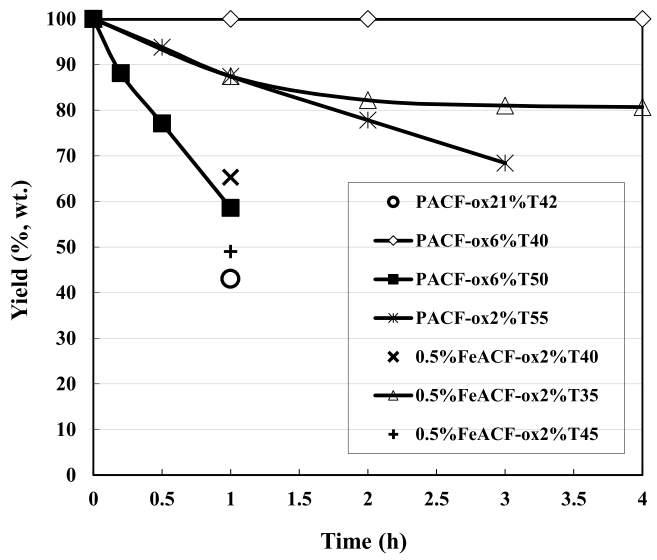

Fig. 2. Yield of ACF at different oxidation conditions.

the oxidation. On the other hand, PACF oxidized with 6 % O_2 (N_2 base) at 400 °C (PACF-ox6 %T40) shows very little weight change, suggesting the oxidation reactivity is low. However, further increasing the temperature to 500 °C (PACF-ox6 %T50) reduces the weight of ACF enormously. The oxidation rate of ACF was somewhat difficult to control even at an oxygen concentration as low as 6 % vol. However, the oxidation of PACF at 550 °C with 2 % oxygen (PACF-ox2 %T55) showed a moderate decrease in weight loss to achieve an average oxidation rate of about 1.8 mg/min. Such a slow rate did not raise the temperature to provoke the ignition of the PACF. The uniform quality of oxidized ACF was obtained.

FeACF is more reactive than the PACF. At a reaction time of one hour, oxidation of FeACF under 2 % oxygen at 400 °C (FeACF-ox2 % T40) gave a lower yield than that of PACF oxidized at a higher temperature (550 °C). An increase of FeACF oxidation temperature from 400 °C to 450 °C reduces its yield from 65.3 % to 49 %, and a further increase to above 450 °C releases larger heat, resulting in difficulty in controlling the desired oxidation temperature. The Fe has been reported to catalyze combustion and gasification reactions. An iron catalyst facilitates redox reactions by providing a pathway for electron transfer and oxidation through the redox cycle between Fe^0, Fe^{2+}, and Fe^{3+}. Iron also contributes to increasing the number of active sites [7], increases char surface area, and lowers activation energy [26,27] to enhance the intrinsic catalytic activity for oxidation. Iron also acts as an oxygen carrier to improve the combustion quality of many fuels [28,29].

Since oxidation under 2 % O_2 in N_2 at temperatures of 550 °C for PACF and at 300 to 450 °C for FeACF showed a moderate decrease in weight loss, therefore to result in a more uniform quality, only oxidized PACF/FeACF produced from the above conditions will be used for the SO_2 removal experiment

3.2. *Characteristics of oxidized ACFs*

3.2.1. *Morphology*

The SEM photographs of PACF, oxidized PACF, and oxidized FeACF can be seen in Fig. 3. The diameter of PACF was about 13 mm. After oxidation to 550 °C for 3 h (PACF-ox2 %T55t3), the diameter decreases to about 8 mm. Meanwhile, the diameter of FeACF after oxidation at 450 °C for 1 h (FeACF-ox2 %T45t1) decreased to about 8 mm to 10 mm and showed a rougher surface. The Fe_2O_3 adhered to the surface of the ACF catalyzes the oxidation reaction locally, creating a rough surface. The existence of Fe_2O_3 adhered to the carbon surface [30]. However, the fate of pitch-based ACF after oxidation with O_2 depends on oxidation conditions. Kaneko et al. reported no change in the ACF morphology even when it was oxidized at 1173 K under an ambient atmosphere [13]. In contrast, Wang et al. oxidized pitch-based ACF under the flow of air at 873 K for one hour and suffered a complete loss of carbon during oxidation [14]. The above report emphasizes the need to optimize oxidation conditions and a low concentration of O_2 gas (O_2 of 2 %) to control the oxidation rate.

3.2.2. *Yield of oxidized ACF after heat treatment*

Weight loss after heat treatment indicates the amount of O_2 content in ACF since O_2 compounds are mainly evaporated during heat treatment. The more weight loss after heat treatment, the more oxygen is incorporated into ACF during oxidation. The weight loss of ACF after heat treatment under an inert atmosphere using a tube furnace can be seen in Table 2. FeACF achieved a higher quantity of weight loss at lower oxidation temperatures than PACF due to the catalytic effect of Fe. Oxidation of the FeACF at temperatures of 400 °C for 1 h (FeACF-ox2 % T40t1) achieved 17.7 % weight loss, which is higher than the weight loss of PACF oxidized at higher temperatures (550 °C) at the same oxidation time. Fe is well known for catalyzing oxidation reactions by decreasing the oxidation temperature.

The weight loss during heat treatment increases with both oxidation temperature and time. However, higher oxygen content will accelerate the burning activity of the carbon. It evaporates oxygen compounds previously introduced to the carbon. Temperature and time for oxidation should be optimized. In this study, the burning event was avoided

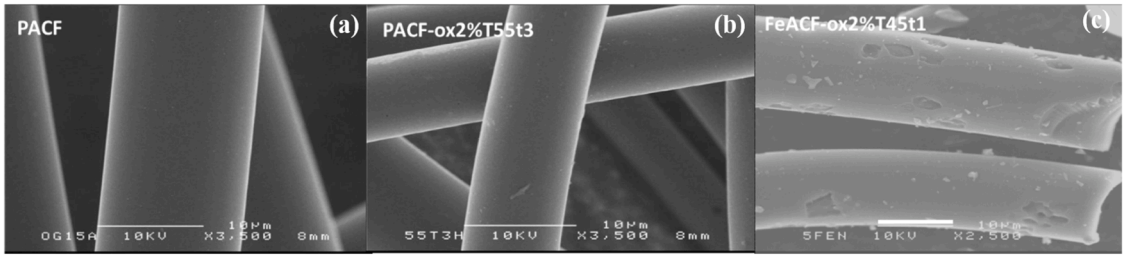

Fig. 3. SEM pictures of (a) ACF, (b) PACF-ox2 %T55t3, and (c) FEACF-ox2 %T45t1.

Table 2
Weight loss of ACF and FeACF after heat treatment at 1100 °C.

ACF samples	Weight loss (%)	FeACF samples	Weight loss (%)
PACF	7.0	FeACF-ox2 %T30t1	7.5
PACF-ox2 %T55t0.5	11.0	FeACF-ox2 %T35t1	14.1
PACF-ox2 %T55t1	14.4	FeACF-ox2 %T40t1	17.7
PACF-ox2 %T55t2	19.9	FeACF-ox2 %T45t1	18.0
PACF-ox2 %T55t3	20.8		

by applying a slow oxidation rate to maximize the introduction of O_2 to the sample.

To understand the weight loss profile of oxidized ACF during heat treatments, FeACF-ox2 %T55t3 and FeACF-ox2 %T45t1 were subjected to thermogravimetric analysis under an inert atmosphere. Weight loss profiles of PACF, oxidized PACF, and oxidized FeACF can be seen in Fig. 4. FeACF oxidized at 450 °C (FeACF-ox2 %T45t1) starts to decompose at a temperature of about 300 °C. In contrast, PACF oxidized at 550 °C (PACF-ox2 %T55t3) decomposes at higher temperatures (> 570 °C). Oxidation temperature and Fe in ACF influence the O_2 functional group formed by oxidation, as indicated by their decomposition temperatures. Meanwhile, without oxidation treatment, PACF decomposes at a temperature higher than 650 °C. Oxidation of ACF lowers its decomposition temperature. The total weight loss of PACF-ox2 % T55t3, which was higher than FeACF-ox2 %T45t1, agrees with the result of heat treatment (as seen in Table 2).

3.2.3. *CO and CO_2 desorption profiles*

Oxygen-containing surface functional groups of carbon materials are decomposed by the calcination, giving rise to the evolution of CO, CO_2, and H_2O. TPD technique is often used to quantitatively evaluate the oxygen-containing surface functional groups by measuring CO and CO_2 amounts and their emission profile [31,32]

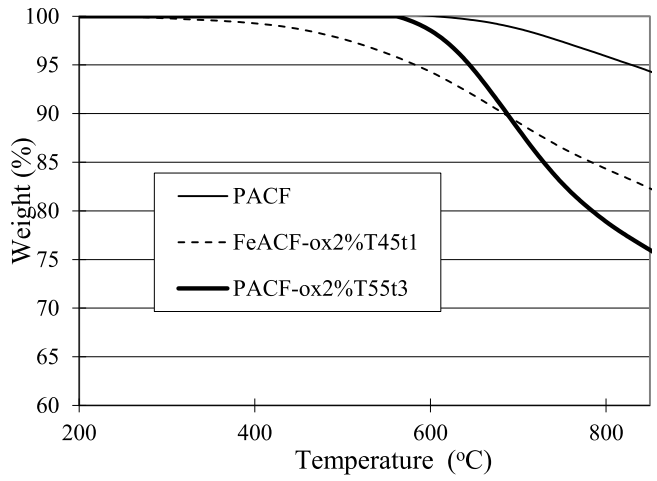

Fig. 4. Thermogravimetric analysis graph of PACF, oxidized PACF, and oxidized FeACF.

CO_2 and CO TPD profiles of ACFs can be seen in Fig. 5. PACF showed a CO_2 desorption peak at about 250 °C. Oxidation treatment shifted the CO_2 desorption peaks to higher temperatures, 326 °C, 572 °C, 660 °C, and 670 °C, for FeACF-ox2 %T35t1, FeACF-ox2 %T45t1, PACF-ox2 % T55t2 and PACF-ox2 %T55t2 respectively. CO_2 desorption at about 250 °C and 400 °C −700 °C was attributed to carboxylic acid and lactone decomposition, respectively [33,34]. On the other hand, the oxidation treatment shifted the CO desorption peak to lower temperatures. The CO desorption peak of PACF, FeACF-ox2 %T35t1, FeACF-ox2 %T45t1, PACF-ox2 %T55t2 and PACF-ox2 %T55t2 were 871 °C, 824 °C, 627 °C, 685 °C and 702 °C, respectively. Oxygen functional groups decomposed to CO at temperatures 700 °C - 900 °C are mainly ethers and carbonyls [33,35].

Oxidation treatment increases the desorption rate of both CO and CO_2. Oxidation of PACF at a temperature of 550 °C for 3 h (PACF-ox2 % T55t3) increased the CO desorption rate from 2.4 mL/min to 5.54 mL/min and the CO_2 desorption rate from 0.16 mL/min to 0.42 mL/min. The CO desorption rate is much larger than CO_2 [36–38]. These results indicate that the low concentration O_2 treatment introduced an abundant amount of oxygen-containing surface functional groups to ACFs.

Two main mechanisms were observed in the formation and decomposition of oxygen groups from modified activated carbon materials. As for samples containing Fe (FeACF), gas release occurred more gradually at medium temperatures (400 °C–600 °C). It indicates that the presence of Fe promotes the formation of new oxygen groups through a redox mechanism, in which Fe^{2+}/Fe^{3+} ions interact with the carbon surface, enabling them to bind and release oxygen in a more controlled manner. Conversely, in the case of samples without Fe (PACF), gas release primarily occurred at high temperatures (650 °C–750 °C) with sharp peaks and greater intensity, indicating the dominance of pure thermal decomposition of oxygen-containing surface functional groups that break down into CO or CO_2. Thus, the Fe-promoted redox-based mechanism resulted in gradual oxygen release, while the pure thermal decomposition mechanism in PACF tended to produce explosive oxygen release at high temperatures [9,39,40].

3.2.4. *Pore structures*

Nitrogen adsorption isotherm and pores distribution of ACFs after oxidation followed by heat treatment can be seen in Fig. 6. The N_2 adsorption isotherms of all ACF samples are of typical type I, indicating the presence of micropores (as seen in Fig. 6**a**). The BET surface area of PACF, FeACF-ox2 %T45t1, and PACF-ox2 %T55t3 are 1520 m^2/g, 1670 m^2/g, and 1750 m^2/g, respectively. Oxidation of ACFs followed by heat treatment increases their surface area. The pore diameter distribution of the ACFs can be seen in Fig. 6**b** Oxidation of PACF at 550 °C for 3 h (PACF-ox2 %T55t3) increased the volume of pores with diameters of about 4.2 nm, 6 nm, and 8 nm −13 nm, while sacrificing smaller pores with diameters of 7 nm and <4 nm. The tiny pores were widened by oxidation. Widening of pores of char/activated carbon due to air oxidation [14,15,41]. Meanwhile, the oxidation of FeACF markedly increases the volume of pores with sizes smaller than 4 nm, indicating iron's role in forming micropores. Such pore structure differences among the ACFs may influence the SO_2 adsorption capacity.

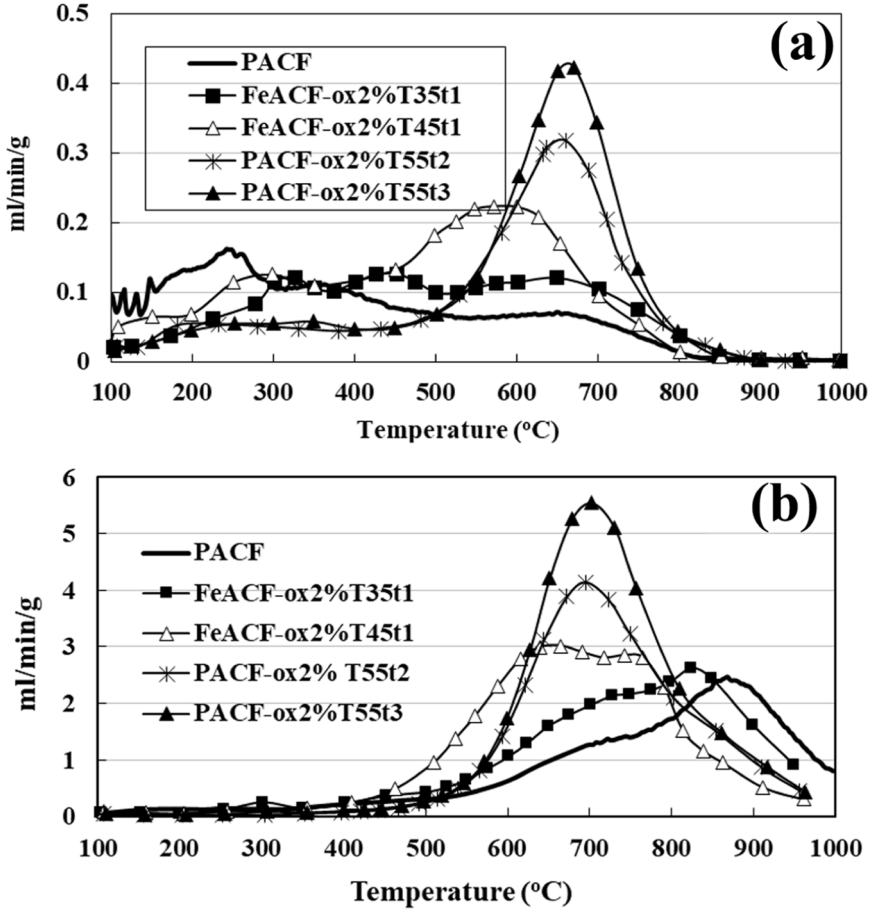

Fig. 5. TPD profiles of (a) CO_2 and (b) CO for PACF, oxidized PACF, and oxidized FeACF.

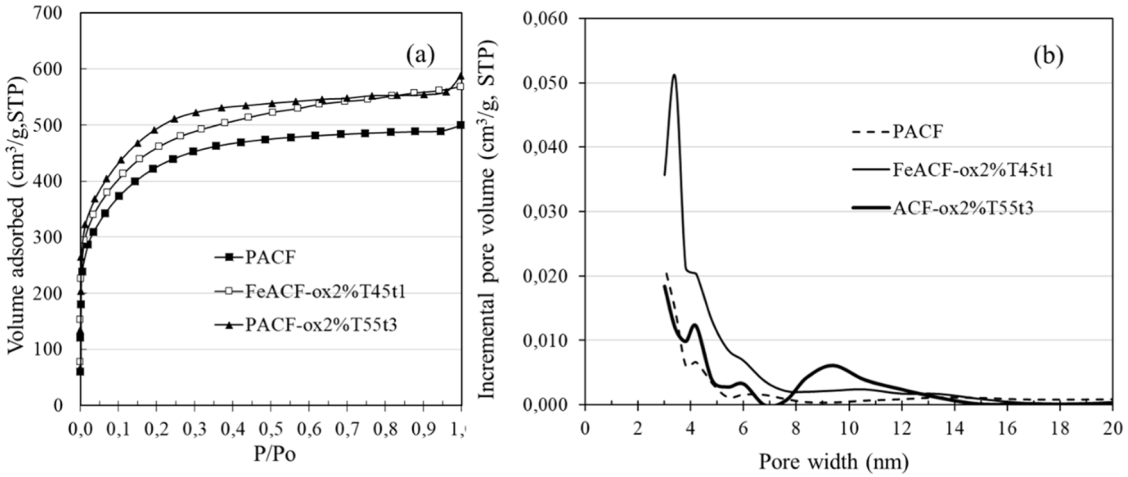

Fig. 6. Nitrogen adsorption isotherm at 77 K and (b) Barrett-Joyner-Halenda (BJH) pore size distribution of pristine and treated ACFs.

3.3. Performance of ACFs for SO_2 removal

The SO_2 removal curves over PACF and oxidized ACF heat treated at 1100 °C can be seen in Fig. 7**a**. SO_2 was initially adsorbed completely in all ACF, and after the breakthrough time, the SO_2 increased rapidly to a stationary concentration. The breakthrough times were 72 min, 77 min, 103 min, 112 min, and 126 min. The stationary concentrations after 15 h were 91 %, 83 %, 75 %, 66 %, 63 % for PACF, PACF-ox2 %T55t0.5, PACF-ox2 %T55t1, PACF-ox2 %T55t2, and PACF-ox2 %T55t3, respectively. Oxidation of the ACF prolonged the breakthrough time and decreased the level of SO_2 stationary concentration. The SO_2 removal curves over PACF and oxidized FeACF can be seen in Fig. 7**b** FeACF-ox2 %T45t1 achieved a breakthrough time of 159 min, which is longer than PACF-ox2 %T55t3 of 126 min (as seen in Fig. 7**a**).

The amount of SO_2 removed for 15 h was estimated by mathematical integration of the SO_2 desulphurization curve in Fig. 7 using a modified Avrami in Eq. (1).

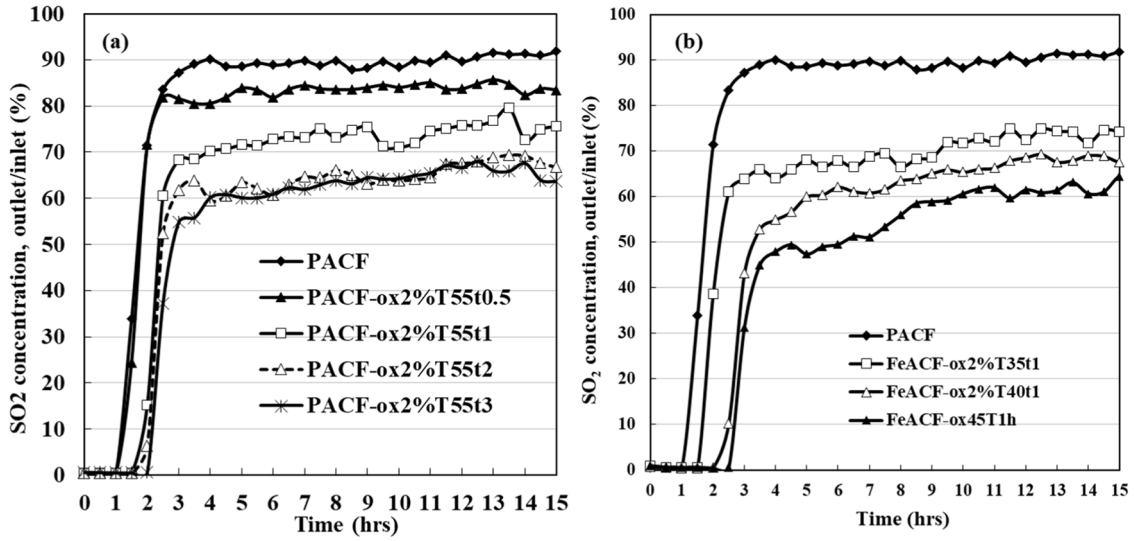

Fig. 7. Influences of oxidation on the desulphurization activity of (a) ACFs and (b) FeACFs.

$$\frac{C_t}{C_i} = \frac{1}{(a + b * \exp(-k * t)} \quad (1)$$

Here, C_t is the SO_2 concentration at time *t*. C_i is an initial concentration of SO_2. The *a, b*, and k values in the equation were obtained through mathematical iteration using Excel Solver software. The SO_2 desulphurization (experimental) curve and the modified Avrami (fitting) curve are presented in Fig. 8. Both curves almost coincide, suggesting that the developed equation is quite accurate for representing the experimental data. The result of the SO_2 removal calculation can be seen in Table 3. Oxidized FeACF achieved the highest SO_2 removal despite its low oxidation temperature. The amount of SO_2 removed by FeACF-ox2 % T45t1 for 15 h was 491 mL/g, more than three times larger than PACF (150.8 mL/g). The ACF treatment by oxidation, followed by calcination, increases ACF removal performance significantly.

The improving performance of ACF after oxidation and calcination may reduce of SO_2 removal cost. The cost of ACF is almost proportional to its surface area because the surface area is proportional to the burn-off amount. Increasing cost due to ACF being burnt during heat treatment may be compensated by the increase adsorption capacity; however, the capital cost of the SO_2 adsorption plant will be reduced due to a smaller volume of adsorption and desorption column required for higher adsorption capacity of ACF. Detailed technoeconomic calculations are required to estimate the cost of desulfurization using ACF.

Table 3
Calculated SO_2 removal amounts for pristine and treated ACFs.

ACF samples	SO_2 removed (mL/g-ACF)	FeACF samples	SO_2 removed (mL/g-FeACF)
PACF	150.8	FeACF-ox2 % T30t1	280.5
ACF-ox2 % T55t0.5	232.7	FeACF-ox2 % T35t1	353.5
ACF-ox2 % T55t1	337.8	FeACF-ox2 % T40t1	431.6
ACF-ox2 % T55t2	406.2	FeACF-ox2 % T45t1	491.0
ACF-ox2 % T55t3	423.6		

The mechanism of SO_2 adsorption on ACF has been explained by several consecutive reactions as follows [42]:

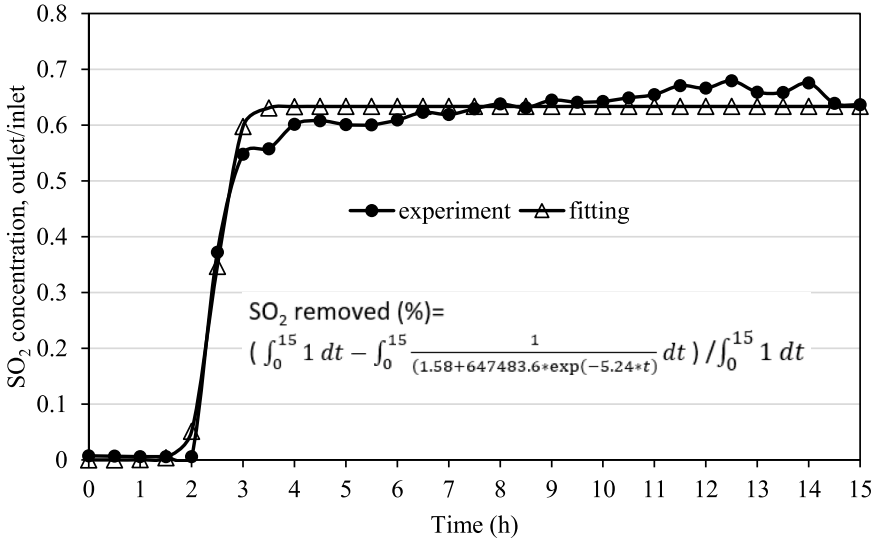

Fig. 8. Comparison of experimental data and fitting curve.

$$SO_2 + \sigma_v \xrightarrow{k_a} SO_2(\text{ads.}) + \sigma_{SO_2} \quad (2)$$

$$SO_2(\text{ads.}) + \sigma_{SO_2} \xrightarrow{O_2} SO_3(\text{ads.}) + \sigma_{SO_3} \quad (3)$$

$$SO_3(\text{ads.}) + \sigma_{SO_3} \xrightarrow{H_2O} H_2SO_4(\text{ads.}) + \sigma_{H_2SO_4} \quad (4)$$

$$H_2SO_4(\text{ads.}) + \sigma_{H_2SO_4} \xrightarrow[k_d]{H_2O} H_2SO_4(\text{aq.}) + \sigma_v \quad (5)$$

The k_a and k_d are the rate constants for adsorption and desorption, respectively. σ_v *is* vacant active sites, and σ_{SO_2}, σ_{SO_3}, and $\sigma_{H_2SO_4}$ denote active sites occupied by SO_2, SO_3, and H_2SO_4, respectively. The suffixes (ads.) and (aq.) indicate adsorbed and dissolved species, respectively.

Initially, SO_2 and O_2 were adsorbed on the vacant active sites of ACF, which were formed through the evolution of CO and CO_2 during heat treatment. The adsorbed SO_2 was oxidized to SO_3, which becomes sulfuric acid by hydration [42,43]. The desorption of H_2SO_4 by H_2O recovers the vacant active site. If the sulfuric acid can be discharged continuously to restore the activity of ACF for SO_2 adsorption, then SO_2 can be removed continuously by ACF.

SO_2 adsorption capacity depends on at least four properties, i.e., micropore volume, pore hierarchy, hydrophobicity, and surface chemistry of ACF. Karatepe et al. investigated the influence of pore parameters on SO_2 adsorption. It found that the micropore volume of the activated carbons, rather than the BET surface area, played an essential role in SO_2 adsorption [44]. Sun et al. emphasize the role of hierarchical pore structure with micropores, mesopores, and/or macropores interconnecting. The micropores serve as gas adsorption and reaction accommodation, and meso-/macropores act as H_2SO_4 transport and buffing reservoirs to give rise to the recovery of active site [45]. The hydrophobicity of the surface also influences the desulfurization activity because the elution of the sulfuric acid from the active site is influenced by the hydrophobicity of the carbon surface. The decomposition of oxygen-containing surface functional groups by the heat treatment modifies the surface chemistry of ACF to influence SO_2 removal activity. Li et al. found that the enhanced activity of SO_2 removal of ACF is proportional to the amount of volatilized CO during heat treatment [24]. Furthermore, Daley et al. found that the amount of volatilized CO_2 correlated with adsorption capacity [20]

This study revealed that oxidation using LOG increased the content of oxygen-containing surface functional groups and specific surface area of ACFs and widened their pore size. The subsequent heat treatment at 1100 °C formed vacant active sites that increase SO_2 adsorption capacity, and improve the hydrophobicity of the ACF surface. A more hydrophobic surface and larger pore diameter increase the elution rate of H_2SO_4, recovering the vacant active site more easily, enabling continuous use of ACF for SO_2 adsorption without regeneration.

Because the specific surface area of ACF was not significantly decreased by the heat treatment at 1100 °C, it is expected that the SO_2 adsorption capacity mainly depends on the number of vacant sites formed by CO and CO_2 evolution during heat treatments and the hydrophobicity of ACF. To clarify the above hypothesis, the weight loss during heat treatment (Table 2) and the amount of SO_2 removed (Table 3) were correlated and presented in Fig. 9. The amount of SO_2 removed is almost linearly correlated with weight loss during heat treatment, indicating both volatilization of CO and CO_2 that influence the activity of ACF. Meanwhile, the higher SO_2 activity of oxidized FeACF than PACF for the same weight loss may be caused by improving the hydrophobicity of FeACF and Fe flexible redox properties. The graphitization near the metal (Fe) may improve hydrophobicity and increase the elution rate of FeACF. Fe is a well-known catalyst for graphitization reactions [46,47]. In addition, the flexible redox properties of Fe enable it to transition between the Fe^{2+} and Fe^{3+} valence states easily. When SO_2 is adsorbed onto the surface, Fe^{3+} ions can oxidize SO_2 into SO_3 while reducing themselves to Fe^{2+} [48,49]. Thus, Fe-doped ACF enhances SO_2 adsorption.

4. Conclusions

Pitch-based ACFs were successfully oxidized using low oxygen gas (2 % O_2 in N_2) without ignition to improve their SO_2 adsorption capacity. The main conclusions are summarized as follows:

- FeACF should be oxidized at a lower temperature than PACF due to the catalytic activity of iron
- The diameter of oxidized ACF is smaller than that of pristine ACF, which allows controlling the ACF diameter by oxidation.
- Higher oxidation temperature yields oxidized ACF of higher decomposition temperature.
- Oxidation increases the number of CO and CO_2 released during heat treatment.
- Oxidation followed by heat treatment increases surface area and widens the pore size of ACF.

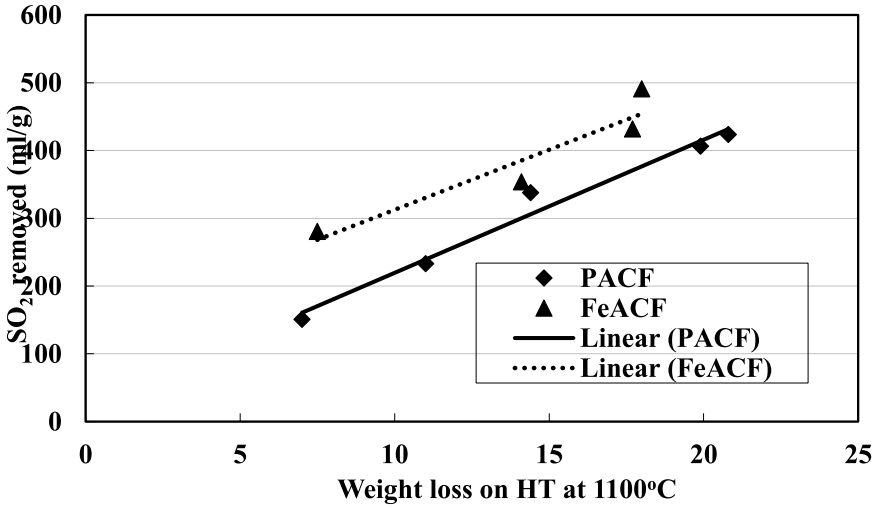

Fig. 9. Correlation between weight loss in the heat treatment and converted SO_2 at a reaction time of 15 h.

- SO_2 removal capacity correlated with weight loss after heat treatment, and FeACF achieved the most significant capacity improvement.

CRediT authorship contribution statement

Miftahul Huda: Writing – original draft, Methodology, Investigation, Data curation, Conceptualization. **Ika Monika:** Formal analysis, Data curation. **Suganal Suganal:** Investigation, Data curation. **Amru Daulay:** Writing – review & editing. **Edwin Akhdiat Daranin:** Visualization, Conceptualization. **Teuku Ishlah:** Writing – review & editing. **Jin Miyawaki:** Writing – review & editing, Supervision.

Declaration of competing interest

The authors declare that they have no known competing financial interests or personal relationships that could have appeared to influence the work reported in this paper.

Acknowledgement

This work was partly supported by the Japanese government scholarship program “Monbukagakusho.”

Data availability

No data was used for the research described in the article.

References

[1] O. Vojáček, J. Brabec, J. Macháč, Costs of achieving emission limits in coal-burning power plants under the recent best available techniques regulation amendment: evidence from national microeconomic data, J. Clean. Prod. 352 (2022) 131600, https://doi.org/10.1016/j.jclepro.2022.131600.

[2] J. Zhang, Y. Zhang, H. Yang, C. Zheng, K. Jin, X. Wu, X. Gao, K. Cen, Cost-effectiveness optimization for SO_2 emissions control from coal-fired power plants on a national scale: a case study in China, J. Clean. Prod. 165 (2017) 1005–1012, https://doi.org/10.1016/j.jclepro.2017.07.046.

[3] W. Wen, C. Wen, D. Wang, G. Zhu, J. Yu, P. Ling, M. Xu, T. Liu, A review on activated coke for removing flue gas pollutants (SO_2, NOx, HgO, and VOCs): preparation, activation, modification, and engineering applications, J. Environ. Chem. Eng. 12 (2024) 111964, https://doi.org/10.1016/j.jece.2024.111964.

[4] Y. Hou, Y. Chen, X. He, F. Wang, Q. Cai, B. Shen, Insights into the adsorption of CO2, SO2 and NOx in flue gas by carbon materials: a critical review, Chem. Eng. J. 490 (2024) 151424, https://doi.org/10.1016/j.cej.2024.151424.

[5] Y. Dong, Y. Li, L. Zhang, L. Cui, B. Zhang, Y. Dong, Novel method of ultralow SO_2 emission for CFB boilers: combination of limestone injection and activated carbon adsorption, Energ. Fuels 31 (2017) 11481–11488, https://doi.org/10.1021/acs.energyfuels.7b01895.

[6] I. Mochida, T. Hirayama, S. Kisamori, S. Kawano, H. Fujitsu, Marked increase of sulfur dioxide removal ability of poly(acrylonitrile)-based active carbon fiber by heat treatment at elevated temperatures, Langmuir 8 (1992) 2290–2294, https://doi.org/10.1021/la00045a036.

[7] M. Liu, Z. Liu, W. Chen, Z. Liu, Z. Li, X. Pi, Q. Du, X. Lai, Y. Xia, Y. Li, NiFe nanoparticle-encapsulated ultrahigh-oxygen-doped carbon layers as bifunctional electrocatalysts for rechargeable Zn−air batteries, Inorg Chem. 62 (28) (2023) 11199–11206, https://doi.org/10.1021/acs.inorgchem.3c01375.

[8] W. Chen, X. Pi, Z. Qu, Y. Li, J. Li, Z. Li, Q. Du, X. Lai, Y. Xia, F. Sun, Pyridinic N–B pair-doped carbon microspheres with refined hierarchical architectures for rechargeable zinc-air batteries, Appl. Energ. 377 (2025) 124511, https://doi.org/10.1016/j.apenergy.2024.124511.

[9] J. Li, W. Chen, X. Pi, Z.J. Liu, X. Song, K. Yang, Y. Li, N-doped pitch assisted local interface micro-environment tailoring and microcrystalline regulation in carbon nanotube for efficient oxygen reduction reaction, https://doi.org/10.1016/j.fuel.2024.133014.

[10] J. Jaramillo, P.M. Álvarez, V. Gómez-Serrano, Oxidation of activated carbon by dry and wet methods, Fuel Process. Technol. 91 (2010) 1768–1775, https://doi.org/10.1016/j.fuproc.2010.07.018.

[11] J.B. Parra, J.J. Pis, J.C. De Sousa, J.A. Pajares, R.C. Bansal, Effect of coal preoxidation on the development of microporosity in activated carbons, Carbon N. Y. 34 (1996) 783–787, https://doi.org/10.1016/0008-6223(96)00030-9.

[12] C.L. Mangun, K.R. Benak, M.A. Daley, J. Economy, Oxidation of activated carbon fibers: effect on pore size, surface chemistry, and adsorption properties, Chem. Mater. 11 (1999) 3476–3483, https://doi.org/10.1021/cm990123m.

[13] K. Kaneko, T. Katori, K. Shimizu, N. Shindo, T. Maeda, Changes in the molecular adsorption properties of pitch-based activated carbon fibres by air oxidation, J. Chem. Soc. Faraday Trans. 88 (1992) 1305, https://doi.org/10.1039/ft9928801305.

[14] Z.-M. Wang, N. Yamashita, Z.-X. Wang, K. Hoshinoo, H. Kanoh, Air oxidation effects on microporosity, surface property, and CH_4 adsorptivity of pitch-based activated carbon fibers, J. Colloid Interface Sci. 276 (2004) 143–150, https://doi.org/10.1016/j.jcis.2004.03.017.

[15] F. Xiao, A.H. Bedane, S. Mallula, P.C. Sasi, A. Alinezhad, D. Soli, Z.M. Hagen, M. D. Mann, Production of granular activated carbon by thermal air oxidation of biomass charcoal/biochar for water treatment in rural communities: a mechanistic investigation, Chem. Eng. J. Adv. 4 (2020) 100035, https://doi.org/10.1016/j.ceja.2020.100035.

[16] H. Rong, Z. Ryu, J. Zheng, Y. Zhang, Effect of air oxidation of Rayon-based activated carbon fibers on the adsorption behavior for formaldehyde, Carbon N. Y. 40 (2002) 2291–2300, https://doi.org/10.1016/S0008-6223(02)00109-4.

[17] C. Moreno-Castilla, F. Carrasco-marín, F.J. Maldonado-hódar, J. Rivera-Utrilla, Effects of non-oxidant and oxidant acid treatments on the surface properties of an activated carbon with very low ash content, Carbon N. Y. 36 (1998) 145–151, https://doi.org/10.1016/S0008-6223(97)00171-1.

[18] A.N.A. El-Hendawy, Influence of HNO_3 oxidation on the structure and adsorptive properties of corncob-based activated carbon, Carbon N. Y. 41 (2003) 713–722, https://doi.org/10.1016/S0008-6223(03)00029-0.

[19] Z. Du, Z. Lei, H. Yan, D. Wang, J. Wang, J. Yan, Z.-K. Li, H. Shui, S. Ren, Z. Wang, Y. Kong, HNO_3 pre-oxidation-tuned microstructures of porous carbon derived from high-sulfur coal for enhancing capture and catalytic conversion of polysulfides, Fuel 326 (2022) 125066, https://doi.org/10.1016/j.fuel.2022.125066.

[20] M.A. Daley, C.L. Mangun, J.A. De Barrb, S. Riha, A.A. Lizzio, G.L. Donnals, J. Economy, Adsorption of SO_2 onto oxidized and heat-treated activated carbon fibers (ACFs), Carbon N. Y. 35 (1997) 411–417, https://doi.org/10.1016/S0008-6223(97)89612-1.

[21] M. Huda, Y. Korai, I. Mochida, Reactivities of Blair Athol and Nang Tong coals in relation to their behavior in PFBC boiler, Fuel 83 (2004) 2151–2156, https://doi.org/10.1016/j.fuel.2004.06.020.

[22] I. Mochida, K. Kuroda, S. Miyamoto, C. Sotowa, Y. Korai, S. Kawano, K. Sakanishi, A. Yasutake, M. Yoshikawa, Remarkable catalytic activity of calcined pitch based activated carbon fiber for oxidative removal of SO_2 as aqueous H_2SO_4, Energ. Fuels 11 (1997) 272–276, https://doi.org/10.1021/ef960160p.

[23] L. Ling, K. Li, L. Liu, S. Miyamoto, Y. Korai, S. Kawano, I. Mochida, Removal of SO_2 over ethylene tar pitch and cellulose-based activated carbon fibers, Carbon N. Y. 37 (1999) 499–504, https://doi.org/10.1016/S0008-6223(98)00219-X.

[24] K. Li, L. Ling, C. Lu, Z. Liu, L. Liu, I. Mochida, Influence of CO-evolving groups on the activity of activated carbon fiber for SO_2 removal, Fuel Process. Techn. 70 (2001) 151–158, https://doi.org/10.1016/S0378-3820(01)00175-8.

[25] A. Islam, S.H. Teo, C.H. Ng, Y.H. Taufiq-Yap, S.Y.T. Choong, M.R. Awual, Progress in recent sustainable materials for greenhouse gas (NOx and SOx) emission mitigation, Prog. Mater. Sci. 132 (2023) 101033, https://doi.org/10.1016/j.pmatsci.2022.101033.

[26] F. Zhang, D. Xu, Y. Wang, M.D. Argyle, M. Fan, CO_2 gasification of Powder River Basin coal catalyzed by a cost-effective and environmentally friendly iron catalyst, Appl. Energy 145 (2015) 295–305, https://doi.org/10.1016/j.apenergy.2015.01.098.

[27] S. Kumar, Y. He, F. Mahmood, Y. Zhu, J. Liu, Z. Wang, W. Shuang, Catalytic influence of iron oxide (Fe_2O_3) on coal pyrolysis and char combustion at various temperatures, Mater. Today Commun. 39 (2024) 108982, https://doi.org/10.1016/j.mtcomm.2024.108982.

[28] X. Zhang, X. Song, J. Wang, W. Su, Y. Bai, B. Zhou, G. Yu, CO_2 gasification of Yangchangwan coal catalyzed by iron-based waste catalyst from indirect coal-liquefaction plant, Fuel 285 (2021) 119228, https://doi.org/10.1016/j.fuel.2020.119228.

[29] J. Chojnacki, J. Kielar, W. Kuczyński, T. Najser, L. Kukiełka, J. Frantík, B. Berner, V. Peer, B. Knutel, B. Gaze, Analysis of the effect of Fe_2O_3 addition in the combustion of a wood-based fuel, Materials 15 (2022) 7740, https://doi.org/10.3390/ma15217740.

[30] S. Amelia, R.S. Muflikhah, Role of the concentration of Fe/C catalysts on heterogeneous Fenton degradation of remazol yellow FG, IOP Conf. Ser. Mater. Sci. Eng. 1053 (2021) 12054, https://doi.org/10.1088/1757-899X/1053/1/012054.

[31] J.L. Figueiredo, M.F.R. Pereira, M.M.A. Freitas, J.J.M. Orfao, Modification of the surface chemistry of activated carbons, Carbon N Y 37 (1999) 1379, https://doi.org/10.1016/S0008-6223(98)00333-9. –138.

[32] G.S. Szymanski, Z. Karpinski, S. Biniak, A. Swiatkowski, The effect of the gradual thermal decomposition of surface oxygen species on the chemical and catalytic properties of oxidized activated carbon, Carbon N Y 40 (2002) 2627, https://doi.org/10.1016/S0008-6223(02)00188-4. –263.

[33] T. Ishii, T. Kyotani, Temperature programmed desorption. Mater. Sci. Eng. Carbon, Elsevier, 2016, pp. 287–305, https://doi.org/10.1016/B978-0-12-805256-3.00014-3.

[34] R. Bavisotto, R. Rana, N. Hopper, K. Hou, W.T. Tysoe, Influence of the terminal group on the thermal decomposition reactions of carboxylic acids on copper: nature of the carbonaceous film, Phys. Chem. Chem. Phys. 23 (2021) 17663–17671, https://doi.org/10.1039/D1CP02078A.

[35] J.-H. Kim, S.-H. Kim, B.-J. Kim, H.-M. Lee, Effects of oxygen-containing functional groups on the electrochemical performance of activated carbon for EDLCs, Nanomaterials 13 (2023) 262, https://doi.org/10.3390/nano13020262.

[36] L. Ling, K. Li, L. Liu, S. Miyamoto, Y. Korai, S. Kawano, I. Mochida, Removal of SO_2 over ethylene tar pitch and cellulose-based activated carbon fibers, Carbon N. Y. 37 (1999) 499–504, https://doi.org/10.1016/S0008-6223(98)00219-X.

[37] J. García-Martín, R. López-Garzón, M.L. Godino-Salido, M.D. Gutiérrez-Valero, P. Arranz-Mascarós, R. Cuesta, F. Carrasco-Marín, Ligand adsorption on an activated carbon for the removal of chromate ions from aqueous solutions, Langmuir 21 (2005) 6908–6914, https://doi.org/10.1021/la050549h.
[38] D. Ibrahim Abouelamaiem, M.J. Mostazo-López, G. He, D. Patel, T.P. Neville, I. P. Parkin, D. Lozano-Castelló, E. Morallón, D. Cazorla-Amorós, A.B. Jorge, R. Wang, S. Ji, M.-M. Titirici, P.R. Shearing, D.J.L. Brett, New insights into the electrochemical behaviour of porous carbon electrodes for supercapacitors, J. Energy Storag. 19 (2018) 337–347, https://doi.org/10.1016/j.est.2018.08.014.
[39] R. Watanabe, P. Verma, H. Akama, C. Fukuhara, Redox mechanism by lattice sulphur in an Fe-based catalyst for propane dehydrogenation with H 2 S co-feeding, RSC Sustain. (2025), https://doi.org/10.1039/D5SU00447K.
[40] X. Zhang, A.C.K. Yip, S. Rosas, M. Nusheh, S. Pang, Enhanced redox performance of cement-modified Fe-based oxygen carrier during biomass chemical looping gasification, Energy 320 (2025) 135393, https://doi.org/10.1016/j.energy.2025.135393.
[41] L. Li, F. Sun, J. Gao, L. Wang, X. Pi, G. Zhao, Broadening the pore size of coal-based activated carbon via a washing-free chem-physical activation method for high-capacity dye adsorption, RSC Adv. 8 (2018) 14488–14499, https://doi.org/10.1039/C8RA02127A.
[42] I. Mochida, K. Kuroda, S. Kawano, Y. Matsumura, M. Yoshikawa, Kinetic study of the continuous removal of SOx on polyacrylonitrile-based activated carbon fibres: 1. Catalytic activity of PAN-ACF heat-treated at 800 °C, Fuel 76 (1997) 533–536, https://doi.org/10.1016/S0016-2361(97)00021-5.
[43] I. Mochida, Y. Korai, M. Shirahama, S. Kawano, T. Hada, Y. Seo, et al., Removal of SOx and NOx over activated carbon fibers, Carbon N. Y. 38 (2000) 227–239, https://doi.org/10.1016/S0008-6223(99)00179-7.
[44] N. Karatepe, I. Orbak, R. Yavuz, A. Özyuguran, Sulfur dioxide adsorption by activated carbons having different textural and chemical properties, Fuel 87 (2008) 3207–3215, https://doi.org/10.1016/j.fuel.2008.06.002.
[45] F. Sun, J. Gao, X. Liu, X. Tang, S. Wu, A systematic investigation of SO_2 removal dynamics by coal-based activated cokes: the synergic enhancement effect of hierarchical pore configuration and gas components, Appl. Surf. Sci. 357 (2015) 1895–1901, https://doi.org/10.1016/j.apsusc.2015.09.118.
[46] A. Gomez-Martin, Z. Schnepp, J. Ramirez-Rico, Structural evolution in iron-catalyzed graphitization of hard carbons, Chem. Mater. 33 (2021) 3087–3097, https://doi.org/10.1021/acs.chemmater.0c04385.
[47] R.D. Hunter, J. Ramírez-Rico, Z. Schnepp, Iron-catalyzed graphitization for the synthesis of nanostructured graphitic carbons, J. Mater. Chem. A 10 (2022) 4489–4516, https://doi.org/10.1039/D1TA09654K.
[48] J. Yao, Z. Zhao, L. Yu, J. Huang, S. Shen, S. Zhao, Y. Wu, X. Tian, J. Wang, Q. Xia, Boosting trace SO_2 adsorption and separation performance by the modulation of the SBU metal component of iron-based bimetal MOFs, J. Mater. Chem. A 11 (2023) 14728–14737, https://doi.org/10.1039/D3TA02223D.
[49] L. An, X. Jia, Y. Liu, Adsorption of SO2 molecules on Fe-doped carbon nanotubes: the first principles study, Adsorption. 25 (2019) 217–224, https://doi.org/10.1007/s10450-019-00026-4.